Available online at www.sciencedirect.com

ScienceDirect

Ceramics International 40 (2014) 1503–1512

CERAMICS INTERNATIONAL

www.elsevier.com/locate/ceramint

Phosphate chemical binder as an anti-hydration additive for Al_2O_3–MgO refractory castables

T.M. Souza[a], A.P. Luz[a,*], T. Santos Jr.[a], D.C. Gimenes[a], M.M. Miglioli[a], A.M. Correa[b], V.C. Pandolfelli[a]

[a]Federal University of São Carlos, Materials Engineering Department, Rod. Washington Luiz, Km 235, São Carlos, SP 13565-905, Brazil
[b]Magnesita Refratários S.A., Research and Development Center, Praça Louis Ensch, 240, Contagem, MG 32210-900, Brazil

Received 3 June 2013; received in revised form 5 July 2013; accepted 6 July 2013
Available online 11 July 2013

Abstract

Even though many investigations have focused on describing the kinetics of both MgO hydration and $Mg(OH)_2$ decomposition, few studies have addressed the understanding of the mechanisms to control or to modify the reaction of magnesia with water. Silica is the most applied anti-hydration additive in MgO-containing castables. The use of silico-phosphates (SiO_2 rich and presenting higher reactivity and solubility) seems to be a promising alternative to induce a faster generation of magnesium–silicate–hydrated gels on the MgO grain surface, inhibiting brucite formation. In the present work, the performance of a commercial phosphate chemical binder (combined or not with silica fume) in Al_2O_3–MgO refractory castables and MgO aqueous suspensions was evaluated. Thermodynamic simulations, thermogravimetric measurements, X-ray diffraction, splitting tensile and hot elastic modulus tests were carried out to understand the additive performance and the characterization of the castables properties. According to the simulated Pourbaix diagrams, two different gels [$Mg_3Si_2O_5(OH)_4$ or $Mg_3Si_4O_{10}(OH)_2$] can be formed in the structure of the samples (depending on the Mg:Si molar ratio), halting the MgO hydration. Due to the high amount of MgO (6 wt%) contained in the designed Al_2O_3–MgO castables, the chrysotile-like phase [$Mg_3Si_2O_5(OH)_4$] should be the main compound formed during the refractories' processing. Moreover, the blend of silica fume and the phosphate-based additive consisted of the most effective route to stop the $Mg(OH)_2$ formation so that castables with high flowability, mechanical strength levels and elastic modulus values can be prepared.

Keywords: $Mg(OH)_2$; Phosphate; Castable; Hydration

1. Introduction

The main obstacle for a wider application of magnesia in refractory castables is related to the $Mg(OH)_2$ (brucite) formation, as such transformation leads to processing drawbacks. MgO hydration can affect the castables' properties mainly at three different stages:

(1) placing, as it reduces the working time and induces a fast flow decay of the compositions;
(2) the curing process, because such a reaction is followed by volume expansion [which is associated to the different densities between magnesia ($\rho = 3.5$ g/cm^3) and the magnesium hydroxide ($\rho = 2.4$ g/cm^3)] which will increase the sample's size. The formed brucite is usually not well accommodated by the castable residual porosity causing damage (i.e., cracks or dusting) in the structure; and
(3) the dry-out of the shaped material, as the $Mg(OH)_2$ decomposition increases the porosity level during the first heating stage in the 400–600 °C range, reducing the material's mechanical strength. Explosive spalling can also take place during this step when high heating rates are applied or large samples are dried out. In this case, the high packing density of the castables can result in water vapor entrapment and, consequently, the development of high pressure levels inside the refractory structure might lead to cracking or even explosions [1–3].

*Corresponding author. Tel.: +55 16 33518253; fax: +55 16 33615404.
E-mail addresses: anapaula.light@gmail.com, vicpando@ufscar.br (A.P. Luz).

0272-8842/$ - see front matter © 2013 Elsevier Ltd and Techna Group S.r.l. All rights reserved.
http://dx.doi.org/10.1016/j.ceramint.2013.07.035

In order to control the MgO hydration in refractory castables, various parameters must be considered: the magnesia source (particle size, specific surface area, purity, CaO/SiO_2 ratio, production route, magnesite calcination temperature and others) [4–8], the pH and temperature of the liquid medium [9,10], the interactions of MgO with other castables' raw materials (such as calcium aluminate cement, hydratable alumina and silica fume) and the additives [1,11–17].

As pointed out in work presented in the literature [11–15,18–21], silica is one of the most applied anti-hydration additives in MgO-containing castables due to its low cost and effectiveness. When in contact with MgO and water, SiO_2 tends to react and generate magnesium–silicate–hydrated gels (M–S–H amorphous phases) on the magnesia grains' surface. According to the reaction mechanism proposed by Salomão and Pandolfelli [22], when an amorphous and a high reactive SiO_2 source (such as silica fume) is exposed to high alkaline environments [pH= 10–12, typical for MgO and calcium aluminate cement (CAC)-containing castables], it partially dissolves, leading to the formation of silicic acid. This acid can be attracted to the alkaline brucite layer (coating the MgO particle surfaces) giving rise to a M–S–H one (Fig. 1) [22], which has low solubility in water in alkaline medium and behaves as a hydrophobic barrier that halts the magnesia hydration [22].

Kalousek and Mui [20], on the other hand, reported that the composition of this formed gel varies according to the MgO/SiO_2 molar ratio (M/S), indicating that the first silicate to be formed is always a chrysotile-like compound [$Mg_3Si_2O_5(OH)_4$], stable for M/S values in the range of 1.25–1.5. For suspensions containing high silica content, a talc-like phase [$Mg_3Si_4O_{10}(OH)_2$] is generated after chrysotile and free silica reaction, whereas for high M/S ratios, brucite and $Mg_3Si_2O_5(OH)_4$ co-exist.

Another way to identify which gel compound is formed at $MgO–SiO_2$ interface is by using thermal (TG, DTA, DSC) analyses. Based on the experimental evaluation of $MgO–SiO_2$ aqueous pastes or MgO-containing castables, some authors highlighted that samples containing $Mg_3Si_4O_{10}(OH)_2$ should show a strong endothermic peak between 900 and 1000 °C [20,21,23]. Conversely, compositions comprised by $Mg_3Si_2O_5(OH)_4$ showed an exothermic peak around 820–840 °C due to the formation of enstatite, forsterite and/or free silica [2,20].

A good alternative to enhance the formation of the M–S–H gel phases and better control the brucite formation consists of using silica-based additives that can induce a faster generation of silicic acid [$H_4SiO_{4(aq)}$] in the liquid medium. For instance, there are some sodium magnesium silico-phosphates available that might fulfill this requirement, as they present a high SiO_2 content (close to 70 wt%), greater reactivity and solubility when compared to crystalline or amorphous silica.

If magnesia can be properly incorporated to refractory compositions, either by inhibiting the associated damage or by using its hydration to promote bonding, a new class of castables can be developed [16]. For this reason, there is a continuous search of alternative routes (anti-hydration additives, anti-damage mechanisms, acceleration and morphology changes of $Mg(OH)_2$ crystals, etc. [2,8,10,18,20,22,24]) for the production of large MgO-containing castable pieces (industrial scale) with mechanical strength levels similar or higher than those attained by conventional binders (calcium aluminate cement and hydratable alumina).

Considering these aspects, this work addresses the evaluation of MgO aqueous suspensions and cement-free $Al_2O_3–MgO$ refractory castables containing silica fume and/or a phosphate chemical binder, as additives to control the $Mg(OH)_2$ formation. Selecting

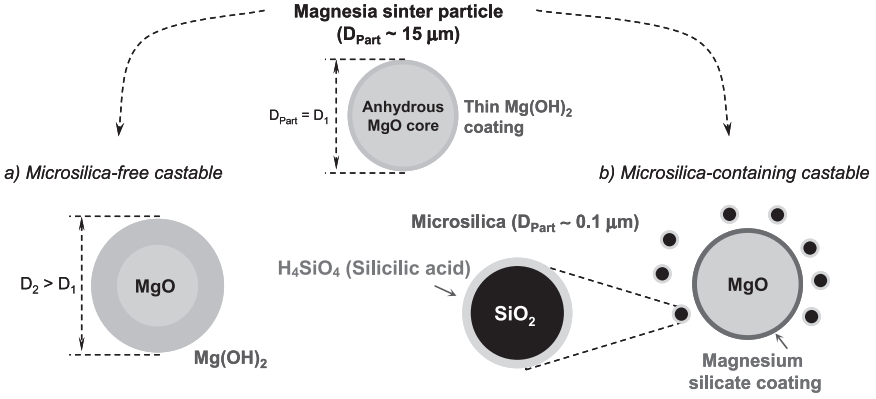

Fig. 1. Sketch of silica's anti-hydration mechanism for magnesia [22].

Table 1
Chemical composition and properties of the chemical binder used in this work.

Additive	Chemical composition (wt%)				pH (1%)	Weight loss (up to 1000 °C, wt%)
	SiO_2	MgO	P_2O_5	Na_2O		
PCB	70.0	12.0	10.0	5.0	~8	4.4

this phosphate-based material aimed to induce a faster generation of the gel-like phases during the sample's processing, inhibiting the brucite formation, as well as increasing the mechanical strength of the designed refractories due to the phase transformations derived from the action of this chemical binder. Thermodynamic simulations, thermogravimetric measurements, X-ray diffraction, splitting tensile and hot elastic modulus tests were carried out for a better understanding of the additives performance and the characterization of the castables' properties.

2. Experimental and calculation procedures

2.1. Materials and thermodynamic calculations

The effect of silica fume (971U, Elkem, Norway) and a sodium magnesium silico-phosphate (Zschimmer & Schwarz GmbH & Co KG, Germany) on the MgO hydration of aqueous suspensions, as well as Al_2O_3–MgO cement-free castable compositions were evaluated. According to Table 1, the selected phosphate chemical binder (PCB) contains approximately 70 wt% of SiO_2 in its composition. Comparing the XRD profiles of plain silica fume and PCB powders (Fig. 2), it can be observed that both materials present a characteristic amorphous profile in the range of $2\theta = 15–35^\circ$. Nevertheless, PCB also showed well defined and intense peaks identified as crystalline MgO. Although Na_2O and P_2O_5 seem to be part of the silicate network, MgO might be added to this material at a certain production stage.

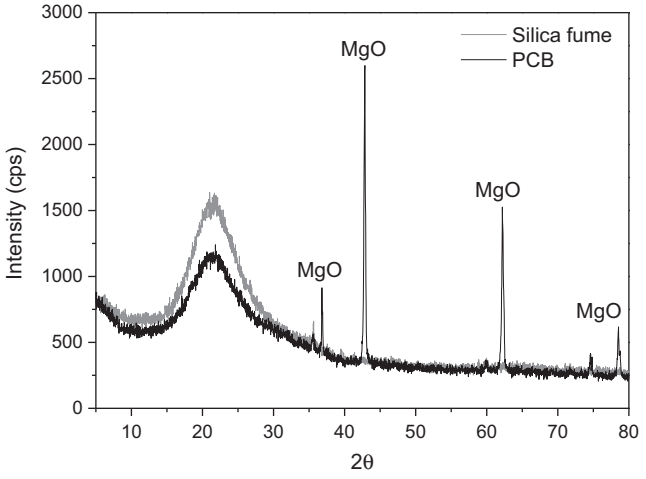

Fig. 2. XRD profiles of the as-received powders of silica fume and the phosphate binder (PCB) [CuKα radiation].

Firstly, aqueous suspensions containing plain MgO (80 wt%) and mixtures of MgO–PCB (6:1 mass ratio) were prepared in order to better verify the anti-hydration effect derived from the action of this additive.

Vibratable alumina–magnesia castable compositions containing silica fume (0, 1 or 2 wt%) with or without PCB (1 wt%) were designed according to Alfred's particle packing model ($q = 0.26$, Table 2) [25]. Coarse tabular alumina was added as aggregates ($d \leq 6$ mm, Almatis, USA) and the matrix fraction comprised magnesia [dead-burnt (DB), $d < 45$ μm, 98.2 wt% of MgO, Magnesita Refratários, Brazil], reactive aluminas (CL370C and CT3000SG, Almatis, USA) and fine tabular alumina (≤200 μm, Almatis, USA). Reference composition without silica fume and PCB (6M0S), as well as an additional high alumina calcium aluminate cement (Secar 71, Kerneos, France) bonded castable (4C2S) were also evaluated. The dispersion of the castables 4C2S, 6M0S and 6M1S was carried out by adding 0.2 wt% of a polycarboxylate based dispersant (Basf, Germany) and 4.0 or 4.5 wt% of water. On the other hand, due to the dispersant action of the phosphate binder, the compositions containing this additive (6M0S-P, 6M1S-P and 6M2S-P) did not require the use of additional agents to attain suitable flowability levels. General information regarding the compositions and the water content required for their appropriate mixing and casting are presented in Table 2. A total of 1 wt% of the PCB was added to the designed compositions comprising 0, 1 or 2 wt% of silica fume.

In order to better understand the dissolution, phase generation and action mechanisms of the phosphate chemical binder during the suspensions and castable preparation at room temperature, Pourbaix diagrams ($E_h \times$ pH) involving Mg, Si, Na, P elements and H_2O were simulated using FactSage™ software (version 6.3.1). EpH module and FactPS and FToxid databases were selected for this evaluation. All diagrams were simulated considering $T = 25\ ^\circ C$ and $m = 10^{-6}$ M (m = aqueous species concentration).

2.2. Experimental tests

Following the mixing step, cylindrical samples (diameter = 20 mm × height = 20 mm) of the aqueous suspensions containing plain MgO (DB) or MgO+PCB (80 wt% of solids) were cast under vibration, kept at 50 °C for 24 h and 110 °C for

Table 2
General information of the designed Al_2O_3–MgO castable compositions.

Raw materials (wt%)	4C2S	6M0S	6M1S	6M0S-P	6M1S-P	6M2S-P
Tabular alumina ($d < 6$ mm)	80.5	87.0	86.0	87.0	86.0	85.0
Reactive aluminas (CT3000SG and CL370C)	13.5	7.0	7.0	7.0	7.0	7.0
Calcium aluminate cement (Secar 71)	4.0	–	–	–	–	–
Silica fume (971U)	2.0	–	1.0	–	1.0	2.0
Magnesia (DB, $d < 212$ μm)	–	6.0	6.0	6.0	6.0	6.0
Phosphate chemical binder (PCB)	–	–	–	1.0	1.0	1.0
H_2O (wt%)	4.5	4.0	4.0	4.5	4.5	4.5

another 24 h. Some cylinders were also fired in electrical furnace (Lindberg Blue, Lindberg Corporation, USA), under a heating rate of 1 °C/min, up to 800 °C and 1000 °C with a dwell time of 5 h. After that, the samples were ground and analyzed by X-ray diffraction and thermogravimetric (TG) techniques. The XRD measurements were carried out in Bruker equipment (model D8 Focus, CuKα radiation [$\lambda = 1.5418$ Å] and nickel filter, using 40 mA, 40 mV and scanning step = 0.02), whereas TG and DSC (differential scanning calorimetry) evaluations of the dried materials were

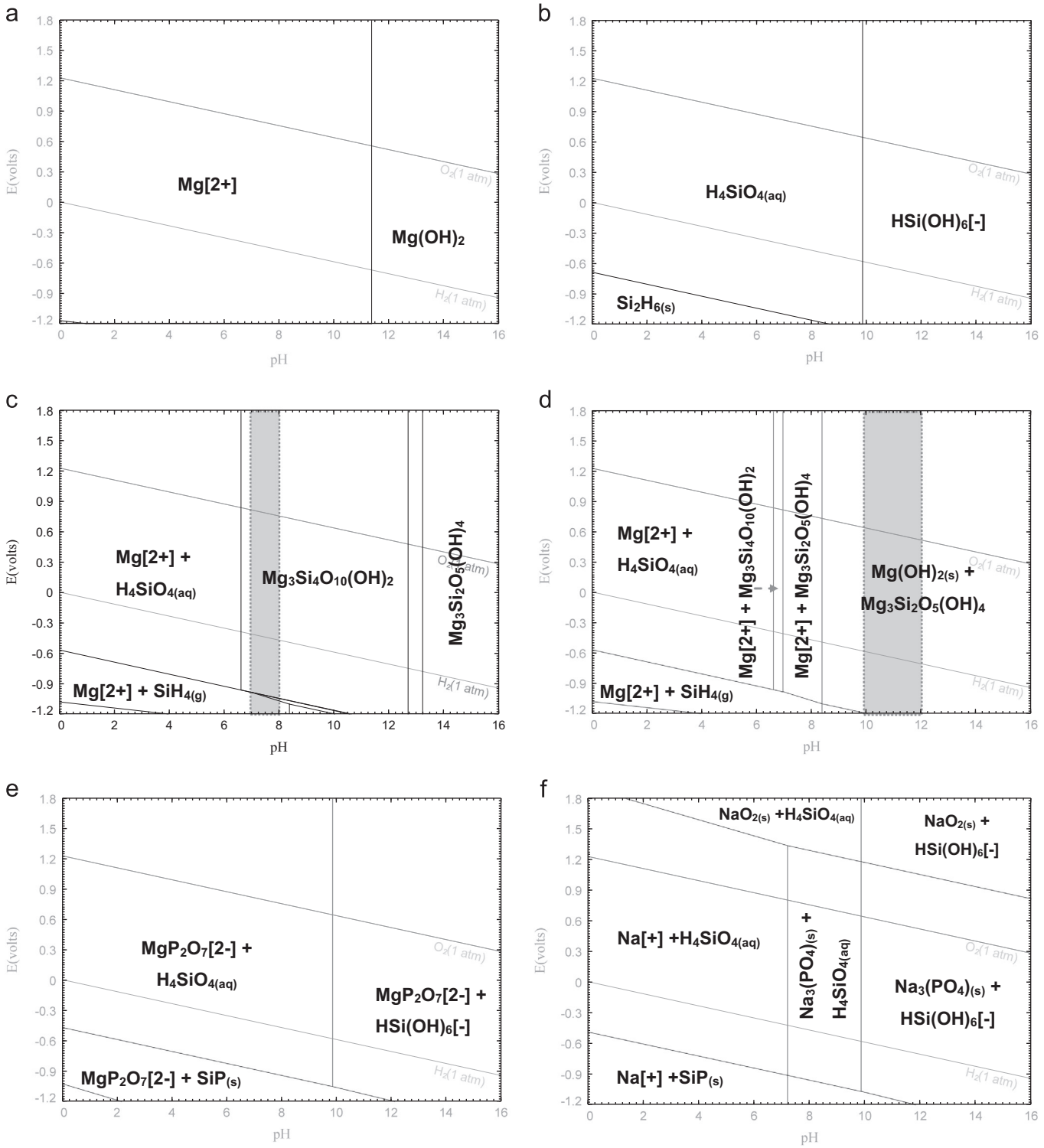

Fig. 3. Pourbaix diagrams ($E \times$ pH) simulated by FactSage™ for $T = 25$ °C. (a) Mg–H_2O, (b) Si–H_2O, (c) Mg–Si–H_2O with Mg:Si < 1 (molar ratio), (d) Mg–Si–H_2O with Mg:Si > 2 (molar ratio), (e) Mg–Si–P–H_2O and (f) Na–Si–P–H_2O. The gray areas highlighted in the (c) and (d) graphs indicate the typical pH values for cement-free suspensions containing the phosphate chemical binder and MgO–containing castables, respectively.

conducted in Netzsch STA 449 equipment, using a heating rate of 10 °C/min with a synthetic air (80% N_2–20% O_2) flow of 50 cm^3/min and α-Al_2O_3 as a correction standard.

On the other hand, during the castable processing step, the compositions were dry-homogenized for 1 min and mixed for an additional 4 min in a rheometer specially developed for refractory castables, by adding the mixing water using a two-step procedure [26]. The castable rheological behavior was evaluated based on flowability tests in a standard flow-table apparatus (ASTM C860).

After that, cylindrical specimens (40 mm × 40 mm) were cast, cured (50 °C/24 h), dried (110 °C/24 h) and fired (200, 600, 800 °C/5 h) for the splitting tensile strength (ASTM C496-90). The mechanical tests were performed in universal mechanical testing equipment (MTS Systems, Model 810, USA) using a constant loading rate of 42 N/s. The splitting tensile strength was calculated by

$$\sigma_f = 2 \times \left(\frac{P}{\pi LD}\right) \quad (1)$$

where σ_f is the splitting tensile stress (MPa), P is the maximum load (N), L (mm) and D (mm) are the height and diameter of the samples, respectively.

Drying tests were carried out up to 750 °C in dried castables (110 °C for 24 h), under a 10 °C min^{-1} heating rate, using a thermogravimetric apparatus designed for the evaluation of large castable samples (diameter = 40 mm and height = 40 mm) [27]. Mass change and the temperature profile of the furnace and of the samples' surface were simultaneously recorded. Percentual mass loss rate (dW/dt, wt%/min) versus samples' temperature was used for the drying behavior evaluation. Furthermore, in order to perform in situ analysis of the microstructural transformations during the first heating up stage of the castables, hot elastic modulus (Scanelastic equipment, ATCP, Brazil) tests were carried out in prismatic samples (150 mm × 25 mm × 25 mm) attained after previous processing steps (curing at 50 °C for 24 h and drying at 110 °C for 24 h). The measurements were conducted using the bar resonance method [28] in the 30–1200 °C range with a heating rate of 2 °C min^{-1}.

3. Results and discussion

3.1. Pourbaix diagrams

In order to understand and explain the behavior of each component contained in the PCB additive when in contact with water, phase diagrams were calculated using the FactSage™ software. Fig. 3 shows the simulated Pourbaix diagrams (E × pH), where the likely stable phases contained in the aqueous electrochemical systems are highlighted. According to these graphs, low E values represent a reducing environment, whereas high E indicates an oxidizing one. Moreover, the area between the two diagonal dashed gray lines shown from the upper left to the lower right in the diagram [pointed out as O_2 (1 atm) and H_2 (1 atm)] is related to the stability field of water at 25 °C.

Fig. 3a and 3b presents the diagrams for the Mg–H_2O and Si–H_2O systems. When contained in an aqueous suspension, Mg can be found dissociated (Mg^{2+}) in the liquid medium (pH < 11.3) or in its hydrated form [$Mg(OH)_2$] in basic conditions (pH > 11.3).

On the other hand, the Si interaction with water should give rise to aqueous silicic acid (H_4SiO_4) or $HSi(OH)_6^-$ ions. Considering that MgO is slightly soluble in aqueous medium [1,5] and correlating the predicted results with the MgO and SiO_2 behavior in water, most likely a $Mg(OH)_2$ layer should be formed on the magnesia solid particles at 25 °C

$$MgO_{(s)} + H_2O \rightarrow Mg(OH)_2 \quad (2)$$

The dissolution of SiO_2 can take place as described in Eq. (3). Nevertheless, the kinetic of this transformation can be strongly affected by [29]: (1) the medium pH and temperature (as shown in Fig. (4)), (2) the silica particle size and its structure (crystalline or amorphous), and (3) the presence of other components in the liquid medium or in the silicate network. According to Iller [29], Si–O–P bonds can be easily hydrolyzed in aqueous solution. This feature might induce a faster formation of $H_4SiO_{4(aq)}$ and, consequently affect the generation of M–S–H phases in suspensions containing MgO and SiO_2

$$SiO_{2(s)} + 2H_2O \rightarrow H_4SiO_{4(aq)} \quad (3)$$

Previous work reported that different gel phases can be formed in aqueous suspensions depending on the MgO and SiO_2 contents [20,23]. For this reason, two diagrams for the Mg–Si–H_2O system were simulated, considering different Mg:Si molar ratios. The PCB additive contains a high amount of SiO_2 (70 wt%) in its composition and the Mg:Si < 1 should better represent the transformations of such material in water (Fig. 3c). Conversely, the suspensions and castable mixes evaluated in this work presented a higher amount of MgO, thus the Mg:Si ratio will be higher than 2 (Fig. 3d). Depending on the pH suspension, the chrysotile-like phase [$Mg_3Si_2O_5(OH)_4$] or the talc-like one [$Mg_3Si_4O_{10}(OH)_2$] might be found and the

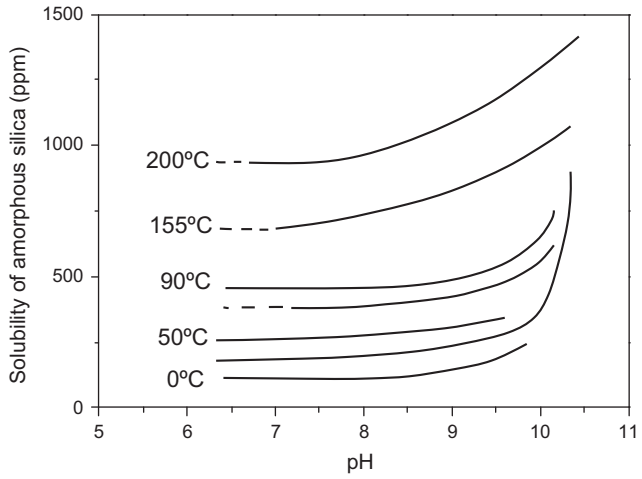

Fig. 4. Solubility of amorphous silica in water as a function of pH at different temperatures [29].

amount of Mg and Si available will induce significant changes in the chemical equilibrium.

Regarding the PCB behavior when mixed with water, this additive should lead to a slightly basic environment (pH between 7.0 and 8.0). The crystalline MgO particles would be partially hydrated, presenting a thin layer of $Mg(OH)_2$ on their surfaces (Eq. (2)). The SiO_2, which is the main component of this material, should be found dissociated in the liquid as $H_4SiO_{4(aq)}$. The combination of brucite and this silicic acid will give rise to $Mg_3Si_4O_{10}(OH)_2$, as shown in Fig. 3c (gray area indicates the typical pH for suspensions containing 1 wt% of the PCB additive) and Eq. (4). This gel phase formed on the MgO particles surface should partly halt the hydration process of this oxide

$$3Mg(OH)_2 + 4H_4SiO_{4(aq)} \rightarrow Mg_3Si_4O_{10}(OH)_2 + 10H_2O \quad (4)$$

On the other hand, the MgO suspensions or Al_2O_3–MgO castable compositions evaluated in this work and containing the selected chemical binder (see Sections 3.2 and 3.3) show a Mg:Si > 2. In this case, the attained pH should be in the range of 10–12 (gray area shown in Fig. 3d). As observed in Fig. 4, faster solubility of silica is expected to take place when the medium pH value is above 9.5. Therefore, when added to MgO-containing castables, silica fume or the silica contained in the PCB additive will be partly dissolved in the liquid medium during the processing step of those materials. The reaction between $Mg(OH)_2$ and $H_4SiO_{4(aq)}$ should lead mainly to the formation of the chrysotile phase [$Mg_3Si_2O_5(OH)_4$, Eq. (5)] instead of the talc-like one. Moreover, due to the limited amount of SiO_2, $Mg(OH)_2$ can still be found in solution. It must be highlighted that the predicted transformations are in agreement with the experimental investigation developed by Kalousek and Mui [20]

$$3Mg(OH)_2 + 2H_4SiO_{4(aq)} \rightarrow Mg_3Si_2O_5(OH)_4 + 5H_2O \quad (5)$$

In addition to MgO and SiO_2, the PCB additive also contains Na_2O and P_2O_5 in its composition (Table 1). Due to the limitations of the FactSage™ software, it was not possible to simulate the Pourbaix diagram for the Mg–Si–Na–P–H_2O system. Nevertheless, the present authors evaluated the Mg–Si–P–H_2O and Na–Si–P–H_2O diagrams in order to check the most likely phases generated due to the interaction of Na and P with the other components in the liquid medium.

Phosphorous should react with Mg resulting $MgP_2O_7^{2-}$ ions in solution (Fig. 3e). Additionally, sodium can also be found dissociated as Na^+ in the suspension or $Na_3(PO_4)_{(s)}$ after its reaction with phosphorous ions (Eq. (6) and Fig. 3f).

$$Na^+ + PO_4^{3-} \rightarrow Na_3(PO_4)_{(s)} \quad (6)$$

Hence, based on the simulated $E \times$ pH diagrams, it was possible to define the reactions sequence and which M–S–H gel phase might be the predominant one [$Mg_3Si_2O_5(OH)_4$ or $Mg_3Si_4O_{10}(OH)_2$] to be formed on the MgO particles surface for different systems (PCB+H_2O or MgO+PCB+H_2O) at 25 °C. Depending on the gel phase contained in the suspension or castable compositions, the molded samples will have their properties affected in different temperature ranges [2,20–23]. More details of the phosphate chemical binder role in halting the MgO hydration are presented as follows.

3.2. Phosphate binder (PCB) anti-hydration performance

Suspensions containing plain dead-burnt MgO or a blend of MgO+PCB (6:1 mass ratio) were prepared, molded as cylindrical samples (d=20 mm and h=20 mm), cured at 50 °C for 24 h, dried at 110 °C for another 24 h and ground before the thermogravimetric measurements (TG/DSC analyses). Fig. 5 shows the drying rate profile as a function of the temperature and the DSC results attained during the tests.

The sample containing plain MgO presented an intense and a well defined peak at 400 °C, which is related to the $Mg(OH)_2$ decomposition (Fig. 5a) during the drying experiment. The MgO+PCB composition, on the other hand, showed a different profile with the presence of two main peaks in the temperature range of 30–250 °C and 250–600 °C in the TG analysis. The first peak seems to be associated to the dehydration of the gel phase (as the samples were previously kept at 110 °C for 24 h to ensure the release of free water), whereas the second one represents the brucite decomposition. The lower intensity of this latter peak highlights the effective performance of the PCB on halting the MgO hydration.

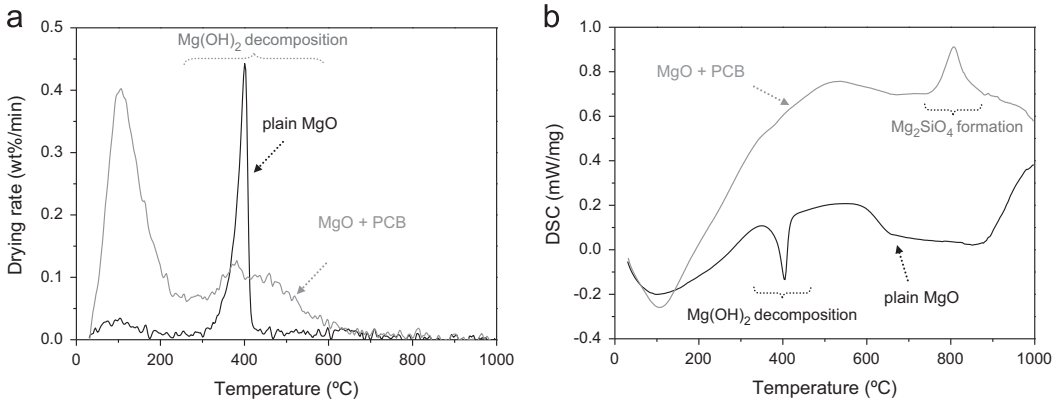

Fig. 5. (a) Drying rate and (b) DSC results as a function of the temperature for samples attained from aqueous suspensions containing plain MgO or MgO+PCB (mass ratio=6:1).

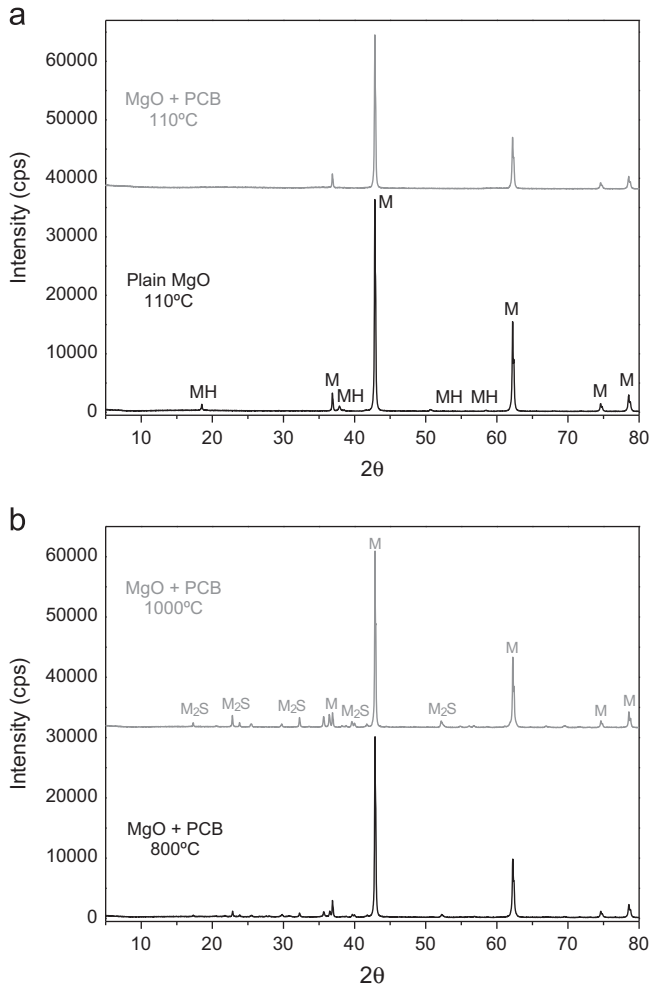

Fig. 6. XRD profiles of the samples attained from aqueous suspensions containing plain MgO or MgO+PCB (mass ratio 6:1), (a) after drying at 110 °C for 24 h and (b) firing at 800 °C and 1000 °C for 5 h. M = MgO, MH = $Mg(OH)_2$ and M_2S = Mg_2SiO_4.

When analyzing the DSC results (Fig. 5b), the M–S–H phase contained in the MgO–PCB sample was identified due to the exothermic peak [characteristic of $Mg_3Si_2O_5(OH)_4$ containing compositions] detected at 808 °C. According to the literature [2,20], the decomposition of the talc-like compound showed no exothermic reaction, but a strong endothermic transformation is commonly detected between 900 and 1000 °C. Hence, as predicted in the Pourbaix diagram (Fig. 3d), only $Mg_3Si_2O_5(OH)_4$ and $Mg(OH)_2$ should be present in the samples containing the sodium magnesium silico-phosphate (PCB) before firing.

Based on Fig. 5b, the endothermic peak associated to the $Mg(OH)_2$ decomposition (~400 °C) was only observed for the plain MgO composition. The XRD profiles illustrated in Fig. 6a (dried powders kept at 110 °C/24 h) also indicated that crystalline brucite was only detected in the additive-free sample. In order to identify which phase transformation was related to the exothermic reaction shown in the DSC measurements, some MgO+PCB samples were also pre-fired at 800 and 1000 °C for 5 h and analyzed via XRD (Fig. 6b). Small peaks of forsterite (Mg_2SiO_4) were identified in the material fired at 800 °C, but the presence of this phase was more evident in the samples attained after firing at a higher temperature (1000 °C).

3.3. Evaluation of cement-free Al_2O_3–MgO castable compositions

Additional experimental measurements (thermogravimetric, flowability, splitting tensile strength and hot elastic modulus tests) were carried out aiming to: (1) compare the efficiency of silica fume and/or the selected PCB additive to halt the MgO hydration, and (2) evaluate their influence on the properties of more complex compositions (i.e., cement-free Al_2O_3–MgO castables).

The reference castable (6M0S) did not contain any source of SiO_2 and, for this reason, a broad and intense decomposition peak (maximum drying rate attained at 442 °C) was observed due to the higher amount of $Mg(OH)_2$ formed in this material (Fig. 7). According to the literature [1,3] brucite starts to thermally decompose at 350–375 °C and above 600 °C no further decomposition should be observed. The addition of 1 wt% of silica fume to the 6M1S castable led to a significant decrease in the drying rate in the 250–470 °C range, which should be related to the anti-hydration role of this amorphous SiO_2 and the resulting lower $Mg(OH)_2$ content.

Despite the higher amount of water (4.5 wt%) required for an appropriate processing and casting of the 6M0S-P samples, this material presented a significant reduction of the brucite decomposition peak (between 350 and 600 °C). Moreover, the maximum drying rate was shifted to a lower temperature (263 °C) and this effect might be associated to the higher content of the chrysotile gel phase generated in this castable. Although this composition contained only 0.7 wt% of SiO_2 (1 wt% of PCB), it is believed that the Si–O–P bonds were easily hydrolyzed, giving rise to a higher amount of $H_4SiO_{4(aq)}$ in the liquid medium and enhancing the M–S–H phase

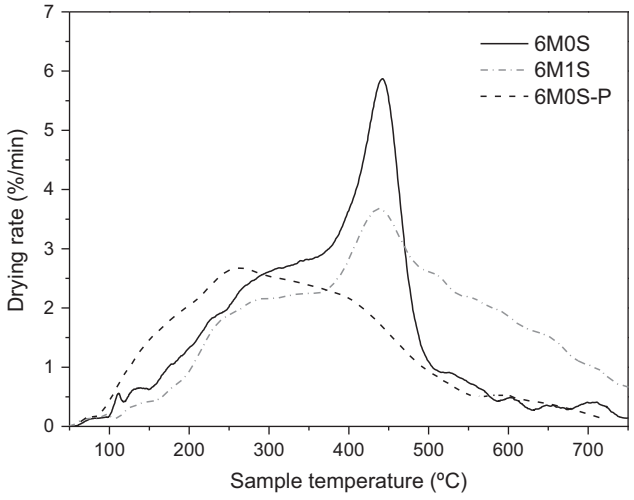

Fig. 7. Drying rate as a function of the temperature of castable samples attained after curing at 50 °C/24 h and drying at 110 °C/24 h.

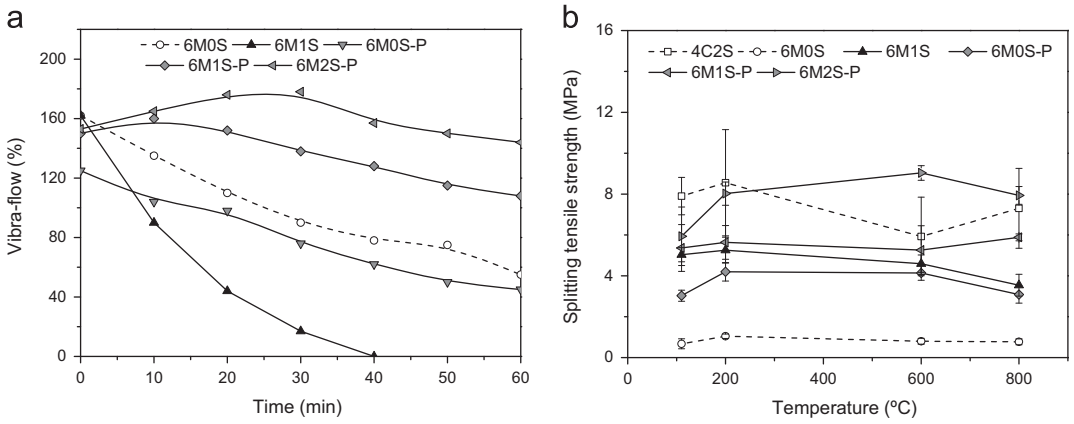

Fig. 8. (a) Vibra-flow (%) as a function of time and (b) splitting tensile strength of dried (110 °C/24 h) and fired castable samples (200 °C, 600 °C and 800 °C for 5 h).

formation. Therefore, the phosphate chemical binder is a more effective anti-hydration additive for MgO-containing castables.

Although some attempts were performed in order to prepare Al_2O_3–MgO castables containing more than 1 wt% of PCB, a fast decay of the flowability levels was noticed and, consequently, the molded samples displayed many surface defects (large pores). For this reason, the present authors decided to only evaluate compositions containing 1 wt% of PCB or a combination of silica fume (1 or 2 wt%)+PCB (1 wt%). Fig. 8a shows the vibra-flow results as a function of time for the designed castables.

When compared to the reference material (6M0S), the addition of 1 wt% of silica fume (6M1S) resulted in a marked decrease of the castable flowability up to 40 min. After that, no flow was observed. On the other hand, the PCB additive did not present a major effect on the castable rheology, as the 6M0S and 6M0S-P compositions showed similar behavior. The blend of SiO_2 and PCB (6M1S-P and 6M2S-P) led to higher flowability levels and increased the castables working time, allowing the preparation of samples with no surface defects and improved finishing. The lubricant effect of silica fume (due to its spherical morphology and small particle size) should be the responsible for the better performance of those refractories and its presence can also favor the packing of particles, filling in the available interstices.

Concerning the mechanical strength of the evaluated compositions, the 6M0S samples (which presented a higher amount of brucite in its structure) showed splitting tensile values in the range of 0.7–1.0 MPa after drying at 110 °C/24 and firing at 200, 600 or 800 °C for 5 h (Fig. 8b). It must be pointed out that the splitting tensile values are equivalent to 1/5 of those attained in cold crushing strength experiments [30]. Nevertheless, this silica-free castable presented a lower mechanical performance when compared to the other Al_2O_3–MgO refractories. Adding 1 wt% of the silica fume (6M1S) or phosphate binder (6M0S-P) induced a 4- or 5-fold increase of the mechanical results. Despite the lower amount of SiO_2 contained in the 6M0S-P composition (0.7 wt%), the enhanced anti-hydration action of the PCB might have helped the good performance presented by this castable. Besides that, after firing at 600 and 800 °C, the attained mechanical strength levels were in the same range (3.0–4.5 MPa) as the ones with 6M1S material. It is important to bear in mind that silica fume addition does not only partly inhibit the magnesia hydration but also improve the packing of particles. Therefore, considering that the PCB addition added less silica to the composition and the particle packing was not benefited, the attained results are considered very promising as the brucite formation was better inhibited.

The combination of PCB and silica fume (6M1S-P and 6M2S-P) led to an improvement of the castable behavior and the fired samples of the composition with higher silica content (6M2S-P, with a total of 2.7 wt% of SiO_2) presented a better mechanical performance even when compared to high alumina cement-bonded castables (reference material, Fig. 8b). Thus, the design of advanced Al_2O_3–MgO cement-free compositions can be accomplished by using appropriate additives to control the brucite formation, allowing the development of refractories with enhanced mechanical strength after firing up to 800 °C.

Aiming to evaluate the phase transformations and their effects on the castables properties, additional *in situ E* analyses up to 1200 °C were carried out for dried samples. Fig. 9 presents the elastic modulus evolution attained during the first thermal cycle, where the results of the reference compositions (4C2S and 6M0S) and the ones for the silica-containing refractories (6M1S, 6M0S-P and 6M2S-P) are shown separately (Fig. 9a and b), in order to see their profiles more clearly.

Due to the higher alumina content, castable 4C2S presented higher initial *E* values (100 GPa) when compared to the Al_2O_3–MgO ones (67–70 GPa). The reference materials featured a characteristic decrease in the elastic modulus in the 120–400 °C (4C2S) and 160–460 °C (6M0S) temperature range due to the cement–hydrates and brucite decomposition, respectively [1,22,27,31]. Moreover, the cement-containing refractory presented an *E* increase between 840 and 1040 °C, pointing out that the sample's densification related to the formation of calcium aluminate phases (CA and/or CA_2). This effect was only observed for the 6M0S at higher temperatures (above 1120 °C, most likely due to the *in situ* $MgAl_2O_4$ formation, Fig. 9a).

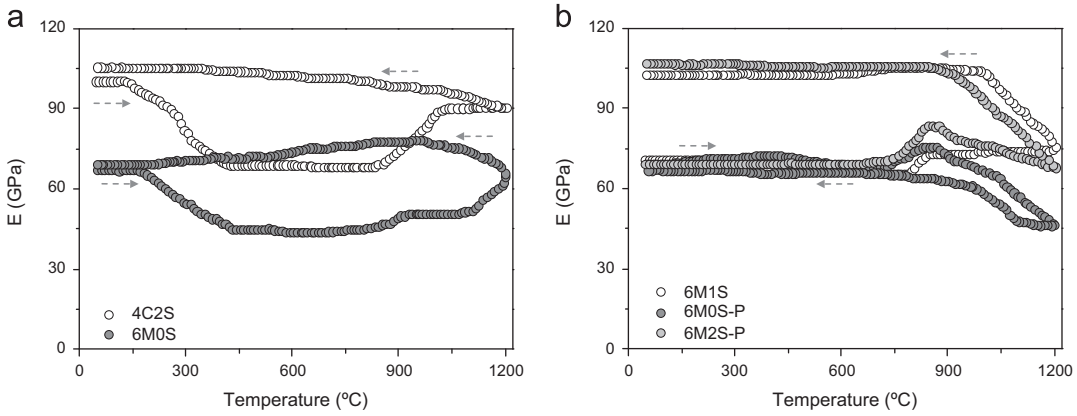

Fig. 9. In situ elastic modulus evolution as a function of the temperature (heating and cooling cycles up to 1200 °C): (a) for the reference compositions [high-alumina calcium aluminate cement-bonded castable (4C2S) and Al_2O_3–MgO silica-free castable (6M0S)], and (b) for the Al_2O_3–MgO castables containing silica fume and/or the phosphate chemical binder (6M1S, 6M0S-P and 6M2S-P). The evaluated samples were previously cured at 50 °C for 24 h and dried at 110 °C for another 24 h.

A slight increase in the *E* values was detected at the beginning of the cooling cycle for both castables due to the material's stiffening [32]. However, the Al_2O_3–MgO composition also showed an *E* decay from 930 °C down to room temperature, as the thermal expansion mismatch of the present phases might have resulted in the generation of microcracks in the castable microstructure. As a consequence, castable 4C2S showed an increase of the samples stiffness (approximately 6%) after the heating–cooling cycle, whereas the 6M0S material kept its final elastic modulus value almost at the same level (69 GPa) as the initial one measured after drying at room temperature.

For the silica-containing Al_2O_3–MgO castables (6M1S, 6M0S-P and 6M2S-P, Fig. 9b), the decrease in the elastic modulus was not observed in the temperature range where the brucite decomposition takes place (350–600 °C) [22]. This fact confirms the effective action of the silica fume and the phosphate binder to halt the $Mg(OH)_2$ formation. 6M1S sample densification started at 780 °C leading to a 14% increase of the *E* value. The same transformation was also observed for the 6M0S-P and 6M2S-P castables, but at earlier temperatures (from 740 up to 870 °C) and was followed by a further decrease in the elastic modulus, which might be related to a liquid phase formation. Based on the DSC and XRD analyses presented in Figs. 5 and 6, it is believed that the forsterite formation (observed in the phosphate containing material) in the samples structure caused the observed *E* increase around 800 °C. Additionally, the presence of the PCB additive seems to affect the samples refractoriness at high temperatures.

The phosphate-containing sample (6M0S-P) showed an increase in its stiffness from 1130 °C down to 650 °C. However, the final elastic modulus attained was very close (67 GPa) to the initial one (69 GPa). The addition of silica fume to the compositions 6M1S and 6M2S-P seems to have a major influence on the samples behavior, mainly at the beginning of the cooling cycle. This *E* variation is related to the usual stiffening of the material when the temperature drops due to the increase in the liquid phase viscosity [32]. Comparing the final elastic modulus (after one thermal cycle) of those samples with the 4C2S, the following sequence was attained: 6M2S-P (107 GPa) > 4C2S (106 GPa) > 6M1S (103 GPa).

4. Conclusions

According to the simulated Pourbaix diagrams, different M–S–H gel phases can be formed [$Mg_3Si_2O_5(OH)_4$ or $Mg_3Si_4O_{10}(OH)_2$] depending on the Mg:Si molar ratio. Due to the high amount of MgO (6 wt%) contained in the designed Al_2O_3–MgO castables or MgO–PCB suspensions, the chrysotile-like phase [$Mg_3Si_2O_5(OH)_4$] should be the main gel phase formed during the refractories' processing. DSC and XRD results confirmed the generation of forsterite (Mg_2SiO_4) at high temperatures (around 800 °C), which is another indicative that $Mg_3Si_2O_5(OH)_4$ was present in the samples' composition.

The phosphate chemical binder evaluated in this work proved to be a more effective anti-hydration additive than silica fume for MgO-containing castables. Although the 6M0S-P contained only 0.7 wt% of SiO_2, it is believed that the Si–O–P bonds were easily hydrolyzed, giving rise to a higher amount of $H_4SiO_{4(aq)}$ in the liquid medium and enhancing the M–S–H phase formation. Some side effects (i.e., fast decay of the castables flowability) were also detected during the preparation of Al_2O_3–MgO castables containing more than 1 wt% of PCB. Therefore, the best alternative to enhance the castables performance was to blend silica fume and this phosphate-based additive. Castable 6M2S-P (which contained a total of 2.7 wt% of SiO_2) showed the best flowability levels and mechanical strength, even when compared with a high alumina cement-bonded castable (4C2S). These results highlighted that the design of advanced Al_2O_3–MgO cement-free compositions can be accomplished by the use of appropriate additives to control the brucite formation, allowing the development of refractories with enhanced mechanical strength after firing at intermediate temperatures (up to 800 °C).

Based on the *in situ* elastic modulus measurements, the presence of the PCB additive seems to affect the samples refractoriness at high temperatures. Considering that the main aim of this publication was to evaluate the use of a more hydrolyzed source of silica to inhibit the brucite formation, this task was attained. Nevertheless, in order to reduce the drawbacks of the selected additive, new ones with high silica and lower sodium contents should be tested.

Acknowledgments

The authors are grateful to CNPq, FIPAI and Magnesita Refratários S.A. for supporting this work.

References

[1] R. Salomão, V.C. Pandolfelli, The role of hydraulic binders on magnesia containing refractory castables: calcium aluminate cement and hydratable alumina, Ceramics International 35 (2009) 3117–3124.
[2] W.M. Silva, C.G. Aneziris, M.A.M. Brito, Effect of alumina and silica on the hydration behavior of magnesia-based refractory castables, Journal of the American Ceramic Society 94 (12) (2011) 4218–4225.
[3] R. Salomão, V.C. Pandolfelli, Magnesia hydration-dehydration behavior in refractory castables, Ceramics International 34 (2008) 1829–1834.
[4] J. Soudier, Understanding and optimization of MgO hydration resistance and spinel formation mechanisms for increasing performance of DVM used in crucible induction furnaces melting steel, in: Proceedings of the Unified International Technical Conference on Refractories (UNITECR), Orlando, USA, 2005.
[5] R.A. Landy, Magnesia refractories, in: C.A. Schacht (Ed.), Refractories Handbook, Marcel Dekker, New York, 2004, pp. 109–149.
[6] V.S.S. Birchal, S.D.F. Rocha, V.S.T. Ciminelli, The effect of magnesite calcinations conditions on magnesia hydration, Minerals Engineering 13 (14 and 15) (2000) 1629–1633.
[7] T. Durán, P. Pena, S. de Aza, J. Gómez-Millán, M. Alvarez, A.H. de Aza, Interactions in calcium aluminate cement (CAC)-based castables containing magnesia. Part I: hydration-dehydration behavior of MgO in the absence of CAC, Journal of the American Ceramic Society 94 (3) (2011) 902–908.
[8] A. Yoshida, T. Nemoto, A. Kaneyasu, Evaluation method for hydration resistance of magnesia fine powder and effect of B_2O_3 content in magnesia raw materials, in: Proceedings of the Unified International Technical Conference on Refractories (UNITECR), Osaka, Japan, 2003, 433-436.
[9] V.A. Phillips, J.L. Kolbe, H. Opperhauser, Effect of pH on the growth of $Mg(OH)_2$ in an aqueous environment at 60 °C, Journal of Crystal Growth 41 (1977) 228–234.
[10] L.F. Amaral, I.R. Oliveira, R. Salomão, E. Frollini, V.C. Pandolfelli, Temperature and common-ion effect on magnesium oxide (MgO) hydration, Ceramics International 36 (2010) 1047–1054.
[11] B. Myhre, B. Sandberg, A.M. Hundere, Castables with MgO–SiO_2–Al_2O_3 as bond phase, in: *Proceedings of the XXVI ALAFAR Congress*, San Juan, Puerto Rico, 1997.
[12] A. Hundere, B. Myhre, C. Odegard, B. Sandberg, N. Zhou, S. Zhang, Z. Bi, Z. Chen, Magnesium-silicate-hydrate bonded MgO–Al_2O_3 castables, in: *38*th *Annual Conference of Metallurgists,* Quebec City, Canada, 1999.
[13] C. Odegard, H. Feldborg, B. Myhre, Magnesia-silica-hydrate bonded MgO castables, in: *Proceedings of the Unified International Technical Conference on Refractories (UNITECR)*, Cancun, Mexico, 2001.
[14] N. Zhou, S. Zhang, S. Hu, Z. Bi, Z. Chen, C. Odegard, B. Myhre, MgO–SiO_2-H_2O bonded castables. Part 2: effect of pumping and wet shotcreting on cold and hot properties and slag resistance, in: *Proceedings of the Unified International Technical Conference on Refractories (UNITECR)*, Osaka, Japan, 2003.
[15] B. Myhre, Cement-free castables in the system MgO–SiO_2: the effect of bond phase modifiers on strength, in: *Proceedings of the 93*th *Annual Meeting of the American Ceramic Society*, Cincinnati, USA, 1991.
[16] T.M. Souza, M.A.L. Braulio, A.P. Luz, P. Bonadia, V.C. Pandolfelli, Systemic analysis of MgO hydration effects on alumina-magnesia refractory castables, Ceramics International 38 (2012) 3969–3976.
[17] T. Durán, P. Pena, S. de Aza, J. Gómez-Millán, M. Alvarez, A.H. de Aza, Interactions in calcium aluminate cement (CAC)-based castables containing magnesia. Part II: hydration-dehydration behavior of CAC and their mixtures with dead-burned and reactive-grade MgO, Journal of the American Ceramic Society 94 (3) (2011) 909–917.
[18] B. Sandberg, T. Mosberg, Use of microsilica in binder systems for ultra-low cement castables and basic, cement-free castables, Ceramic Transactions 4 (1989) 245–258.
[19] J.C. Yang, The system magnesia-silica-water below 300 °C: I. Low-temperature phases formed from 100° to 300 °C and their properties, Journal of the American Ceramic Society 43 (10) (1960) 542–549.
[20] G.L. Kalousek, D. Mui, Studies on formation and recrystallization of intermediate reaction products in the system magnesia-silica-water, Journal of the American Ceramic Society 37 (2) (1954) 38–41.
[21] J. Temuujin, K. Okada, K.J.D. Mackenzie, Role of water in the mechanochemical reactions of MgO–SiO_2 systems, Journal of Solid State Chemistry 138 (1998) 169–177.
[22] R. Salomão, V.C. Pandolfelli, Microsilica addition as an anti-hydration technique for magnesia-containing refractory castables, American Ceramic Society Bulletin 86 (6) (2007) 9301–9306.
[23] J. Szczerba, R. Prorok, E. Sniezek, D. Madej, K. Maslona, Influence of time and temperature on ageing and phases synthesis in the MgO–SiO_2-H_2O system, Thermochimica Acta, (2013), http://dx.doi.org/10.1016/j.tca.2013.01.018.
[24] T.M. Souza, M.A.L. Braulio, V.C. Pandolfelli, Novel technological route to overcome the challenging magnesia hydration of cement-free alumina castables, Refractories World Forum 5 (2013) 94–98.
[25] R.G. Pileggi, F.T. Ramal Jr., A.E.M. Paiva, V.C. Pandolfelli, High performance refractory castables: particle size design, Refractory Applications and News 8 (2003) 17–21.
[26] R.G. Pileggi, V.C. Pandolfelli, A.E.M. Paiva, J. Gallo, Novel rheometer for refractory castables, American Ceramic Society Bulletin 79 (2000) 54–58.
[27] M.D.M. Innocentini, F.A. Cardoso, M.M. Akyioshi, V.C. Pandolfelli, Drying stages during the heating of high-alumina, ultra-low-cement refractory castables, Journal of the American Ceramic Society 86 (7) (2003) 1146–1148.
[28] G. Pickett, Equations for computing elastic constants from flexural and torsional resonant frequencies of vibration of prisms and cylinders, Proceedings: American Society for Testing Materials 45 (1945) 846–865.
[29] R.K. Iller, The chemistry of silica, Solubility, Polymerization, Colloid and Surface Properties, and Biochemistry, John Wiley, New York40–65.
[30] C.R.V. Cruz, Refractories for steelmaking equipments, São Paulo: Associação Brasileira de Metais (1982) 515 (in Portuguese).
[31] A.P. Luz, V.C. Pandolfelli, Halting the calcium aluminate cement hydration process, Ceramics International 37 (2011) 3789–3793.
[32] A.P. Luz, M. Huger, V.C. Pandolfelli, Hot elastic modulus of Al_2O_3–SiC–SiO_2–C castables, Ceramics International 37 (2011) 2334–2345.